



Titre: Single pulse nanosecond laser-stimulated targeted delivery of anti-cancer drugs from hybrid lipid nanoparticles containing 5 nm gold nanoparticles
Title:

Auteurs: Antoine Uzel, Leonidas Agiotis, André Baron, Igor V. Zhigaltsev, Pieter R. Cullis, Morteza Hasanzadeh Kafshgari, & Michel Meunier
Authors:

Date: 2023

Type: Article de revue / Article

Référence: Uzel, A., Agiotis, L., Baron, A., Zhigaltsev, I. V., Cullis, P. R., Kafshgari, M. H., & Meunier, M. (2023). Single pulse nanosecond laser-stimulated targeted delivery of anti-cancer drugs from hybrid lipid nanoparticles containing 5 nm gold nanoparticles. *Small*, 19(52), 2305591 (11 pages).
Citation: <https://doi.org/10.1002/sml.202305591>

 **Document en libre accès dans PolyPublie**
Open Access document in PolyPublie

URL de PolyPublie: <https://publications.polymtl.ca/56707/>
PolyPublie URL:

Version: Version officielle de l'éditeur / Published version
Révisé par les pairs / Refereed

Conditions d'utilisation: CC BY
Terms of Use:

 **Document publié chez l'éditeur officiel**
Document issued by the official publisher

Titre de la revue: Small (vol. 19, no. 52)
Journal Title:

Maison d'édition: Wiley-Blackwell
Publisher:

URL officiel: <https://doi.org/10.1002/sml.202305591>
Official URL:

Mention légale: © 2023 Uzel, A., Agiotis, L., Baron, A., Zhigaltsev, I. V., Cullis, P. R., Kafshgari, M. H., & Meunier, M. Small published by Wiley-VCH GmbH. This is an open access article under the terms of the Creative Commons Attribution License, which permits use, distribution and reproduction in any medium, provided the original work is properly cited.
Legal notice:

Single Pulse Nanosecond Laser-Stimulated Targeted Delivery of Anti-Cancer Drugs from Hybrid Lipid Nanoparticles Containing 5 nm Gold Nanoparticles

Antoine Uzel, Leonidas Agiotis, Amélie Baron, Igor V. Zhigaltsev, Pieter R. Cullis, Morteza Hasanzadeh Kafshgari,* and Michel Meunier*

Encapsulating chemotherapeutic drugs like doxorubicin (DOX) inside lipid nanoparticles (LNPs) can overcome their acute, systematic toxicity. However, a precise drug release at the tumor microenvironment for improving the maximum tolerated dose and reducing side effects has yet to be well-established by implementing a safe stimuli-responsive strategy. This study proposes an integrated nanoscale perforation to trigger DOX release from hybrid plasmonic multilamellar LNPs composed of 5 nm gold (Au) NPs clustered at the internal lamellae interfaces. To promote site-specific DOX release, a single pulse irradiation strategy is developed by taking advantage of the resonant interaction between nanosecond pulsed laser radiation (527 nm) and the plasmon mode of the hybrid nanocarriers. This approach enlarges the amount of DOX in the target cells up to 11-fold compared to conventional DOX-loaded LNPs, leading to significant cancer cell death. The simulation of the pulsed laser interactions of the hybrid nanocarriers suggests a release mechanism mediated by either explosive vaporization of thin water layers adjacent to AuNP clusters or thermo-mechanical decomposition of overheated lipid layers. This simulation indicates an intact DOX integrity following irradiation since the temperature distribution is highly localized around AuNP clusters and highlights a controlled light-triggered drug delivery system.

successfully cure early stage cancers, they pose problems for advanced cancers. In the case of chemotherapy, treatments are long, and because chemotherapeutic agents are not specific to cancer cells, <5% of the anticancer drug reaches the tumor through the bloodstream.^[1] Some chemotherapeutic agents (e.g., DOX)^[2] are also cardiotoxic and accumulate in the patient's heart, limiting the cumulative dose the body can tolerate.^[3] Innovative drugs encapsulated in LNPs to deliver treatments and perform cancer therapy have emerged as new functional strategies. Their effectiveness has been demonstrated, for example, with Covid-19 vaccines.^[4] The lipid bilayer provides a protective barrier against early drug elimination and allows passive delivery of chemotherapeutic agents to the tumor. Encapsulation of the anticancer drug in liposomes, such as Doxil,^[4] reduces toxic side effects. Studies have further shown that it reduces the photodegradation of DOX^[5] and generally promotes the photostability of other photosensitive drugs.^[6] Moreover, the encapsulation of anticancer drugs


1. Introduction

Chemotherapy, surgery, and radiation therapy are standard methods to treat breast cancer. However, while these methods

in liposomes increases tumor accumulation, assisted by the impact of enhanced permeation and retention. Although a significant improvement over chemotherapy alone, lipid encapsulation of cargo has limitations, that is, chemotherapeutic agent release in healthy tissues. Site-specific delivery to minimize collateral damage to healthy tissue can be achieved by triggered release (stimuli-responsive release). For instance, endogenous stimuli, for example, triggered by changes in pH, redox conditions, and enzymes at the diseased site, can be utilized to locally degrade liposomes sensitive to these stimuli.^[7] However, the complexity of the intracellular mechanisms of cancer cells compared to non-cancerous cells or immune reactions to enzymes,^[8] may lead to an ineffective treatment induced by endogenous stimuli.

Alternatively, external stimuli can trigger a remote drug release of stimuli-responsive liposomes accumulated at the tumor site.^[7a,9] These external stimuli include magnetic fields, ultrasound, heat, microwave radiation, and light. Among the various external stimuli available, laser light is an appealing candidate as it generally allows for remote interaction with engineered nanomaterials with high spatiotemporal resolution and

A. Uzel, L. Agiotis, A. Baron, M. Hasanzadeh Kafshgari, M. Meunier
Department of Engineering Physics
Polytechnique Montréal
Montreal, QC H3C 3A7, Canada
E-mail: morteza.kafshgari@tum.de; michel.meunier@polymtl.ca
I. V. Zhigaltsev, P. R. Cullis
Department of Biochemistry and Molecular Biology
University of British Columbia
2350 Health Sciences Mall, Vancouver, BC V6T 1Z3, Canada

 The ORCID identification number(s) for the author(s) of this article can be found under <https://doi.org/10.1002/smll.202305591>

© 2023 The Authors. Small published by Wiley-VCH GmbH. This is an open access article under the terms of the Creative Commons Attribution License, which permits use, distribution and reproduction in any medium, provided the original work is properly cited.

DOI: 10.1002/smll.202305591

spectral selectivity.^[10] Wavelengths in the ultraviolet-visible range are primarily applicable for topical treatments, while the near-infrared range is preferred to obtain penetration depths of a few millimeters and avoid interaction with most biomolecules found in tissue.^[11] For deeper areas of the body, minimally invasive interstitial laser thermal therapy utilizing optical fiber is required. As for the development of compatible, laser light-responsive liposomes, many efforts have been devoted to the incorporation of AuNPs within specified compartments of the liposomes^[12] as well as the other approaches assembling plasmonic NPs within polymer nanostructures.^[13] Indeed, the development of such therapeutic nano-platforms not only facilitates their spectral tunability to the desired laser wavelength (due to the surface plasmon resonance of AuNPs) but also further pushes the precision of the interaction to the nanoscale.^[14] Therefore, such precision enables nanometric manipulation of localized regions on a single liposome.

Over the past decade, various laser radiation approaches (i.e., continuous wave or pulsed) have been employed to trigger cargo release from AuNP-containing liposomes or other polymeric nanovesicles.^[15] Each approach differs regarding underlying mechanisms and cargo release kinetics. To begin with, drug release from AuNP-containing liposomes by continuous wave laser radiation relies on local hyperthermia, increasing the liposome membrane permeability.^[10b] However, by this approach, the release rate of chemotherapeutics can only be reduced to the minute timescale.^[16] Consequently, these conditions do not allow optimal drug concentration at a treated tumor site, highlighting the requirement for a faster release strategy.^[17] Pulsed laser irradiation can address this problem by allowing the decomposition of the liposomes' membranes via a single laser shot.^[17] Release occurs rapidly, ultimately governed by the diffusion of the drug to its surroundings. Specifically for doxorubicin chemotherapy by AuNP-containing liposomes, several approaches for light-triggered release by multiple laser pulses have been proposed.^[18] Other studies have utilized multiple laser pulse triggering for photoacoustic imaging^[19] or DNA plasmid transfection.^[20] Only a few works have examined the effect of content release (e.g., calcein,^[12a,c] calcium,^[12b,21] inositol triphosphate,^[21] adenosine triphosphate,^[12b] or carboxyfluorescein^[12b,d]) from liposome/AuNP carriers by a single laser pulse.^[12a,b,21] Relatively large Au nanostructures (≈ 40 – 50 nm) have been used to manage content release from AuNP-containing liposome vesicles,^[12b-d] presumably via a bubble cavitation process. Other approaches exploit smaller AuNPs (< 5 nm) to cover the liposome membrane and tune the surface plasmon resonance of the vesicles to the near-infrared range so that uncaging of cargo is triggered by either nanobubble formation or mechanical forces.^[12a,21] Still, the underlying mechanisms of single pulse release of chemotherapeutic agents from light-responsive liposomes remain elusive.

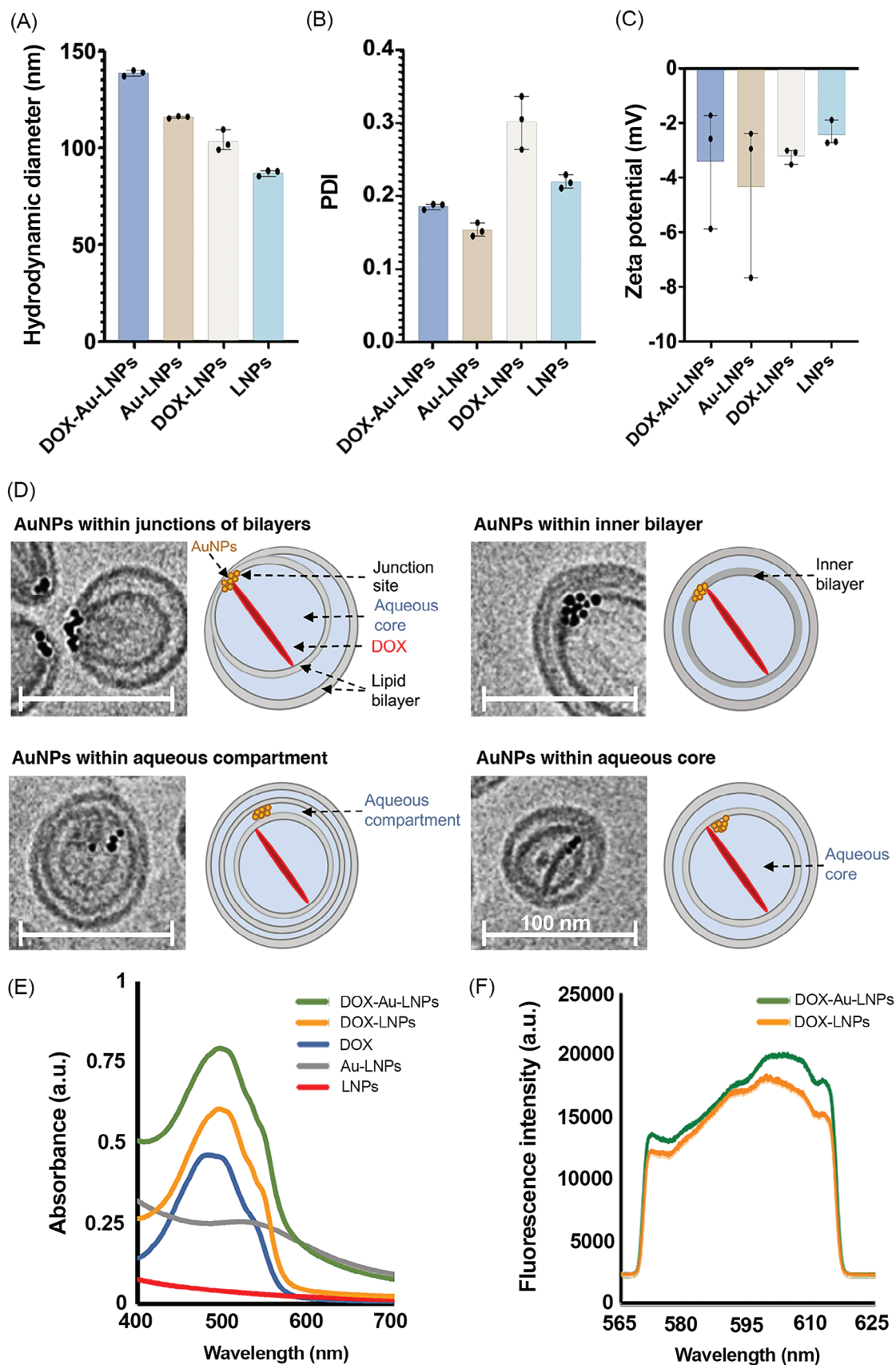
To develop a site-specific stimuli-responsive drug release system, a new generation of light-responsive oligolamellar LNPs containing AuNP clusters inside their membrane (residing within junctions of the lamellae) has been formulated for promoting a safe and controlled chemotherapy. DOX has been tightly encapsulated in the aqueous core of the hybrid plasmonic LNPs and released into the target cancer cells after exposure to the pulsed ns laser. Benefiting from the localized interaction of a well-defined plasmonic resonance (540 nm) of AuNPs with

nanosecond pulsed-laser irradiation at the same resonance peak, we establish site-specific light-triggered delivery of DOX in MDA-MB-231 human breast adenocarcinoma cells by application of a single pulse per irradiated site. Further, a numerical model is developed to shed light on the mechanisms of the triggered drug release from the internalized DOX-Au-LNPs through single-pulsed irradiation to demonstrate the localized stimuli-responsive delivery of LNP-mediated chemotherapy with a fast release rate triggered by a single laser pulse.

2. Results and Discussion

2.1. Formulation of DOX-Loaded Hybrid Plasmonic LNPs

Hybrid plasmonic LNPs have been synthesized by a recently developed “bottom-up” approach^[22] to encapsulate hydrophobic negatively charged AuNPs and DOX, a hydrophilic anticancer drug. The hybrid LNPs are assembled by mixing ionizable cationic lipids (1, 2-dioleoyl-3-dimethylammonium-propane = DODAP) with distearoylphosphatidylcholine (DSPC), cholesterol, and poly(ethylene glycol)-1, 2-distearoyl-sn-glycerol-3-phosphoethanolamine (PEG-DSPE) through a well-established volume ratio of 10/49/40/1 to entrap the negatively charged AuNPs (5 nm in diameter)^[22] within the membrane of LNPs (junction of bilayers). Therefore, the outermost monolayer of the hybrid LNP presented here is composed almost entirely of DSPC and cholesterol to prevent immune responses and provide a longer circulation time. The hybrid plasmonic LNPs have been formulated with an average hydrodynamic diameter of ≈ 138 nm (polydispersity index = PDI of 0.19) and negative zeta potential (-3.4 mV), as shown in **Figure 1A–C**. The AuNP/lipid molecule ratio was 2.2×10^{13} particles/ μmol lipid for forming the Au-LNPs, thereby obtaining AuNP entrapment efficiency close to 100%.^[22] Furthermore, LNP formulations, including DOX-Au-LNPs as well as control Au-free DOX-LNPs, were loaded with DOX by following 0.1 DOX/total lipids ratio (wt/wt) to achieve a loading efficacy $\approx 100\%$, exactly as described in the earlier work.^[22] AuNP clusters have been precisely placed within the junctions of the lipid bilayers (average 5–7 particles per LNP) of these bilamellar or oligolamellar vesicles (**Figure 1D**). Accordingly, the most representative case corresponds to the top-left image, that is, AuNPs are clustered within the junction of lipid bilayers. Note that other structures, such as bilamellar or oligolamellar vesicles, with AuNP clusters placed within i) inner lipid bilayers, ii) intermediate aqueous compartments, or iii) inner aqueous compartments have been observed with less population (**Figure 1D**). However, the entrapped internalized AuNPs are still associated with lipids without being freely dispersed in the aqueous phase since the cationic lipid (DODAP) drives the AuNP uptake upon the formation of the hybrid system. To enable DOX encapsulation in the formulated hybrid plasmonic LNPs, ammonium sulfate was entrapped into the aqueous core by taking advantage of the created pH gradient between the interior of the liposomes and the exterior. In all cases, the DOX encapsulation has occurred in the aqueous core of the vesicles, forming a rod-shaped nanocrystal (**Figure 1D**) with high loading efficiency (an initial drug-to-lipid ratio of 0.1 wt./wt.) without any probable leakages in the physicochemical conditions. The absorbance spectrum of 5 nm AuNPs peaks at 520 nm according to



manufacturer technical data (Ted Pella Inc, 5 nm PELCO NanoX-act Gold Nanoparticles), in fair accordance with Mie theory (plasmon peak at 522 nm for AuNP in water). The formulation of the DOX-loaded hybrid plasmonic LNPs (DOX-Au-LNPs) has been validated by evaluating the ultraviolet–visible spectroscopy (absorbance spectrum) of the encapsulated AuNPs with a plasmon peak at ≈ 540 nm (Figure 1E), whereas absorbance and fluorescence peak of the encapsulated DOX has been observed at ~ 495 and ~ 590 nm (Figure 1E,F). The plasmon peak shift at 540 nm is indicative of aggregation of 5 nm AuNPs within lipids. According to the optical properties of the formulated DOX-Au-LNPs, a pulsed laser with an irradiation peak at ≈ 530 nm would efficiently provide the resonant effect to obtain the stimuli-responsive DOX release.

2.2. Stimuli-Responsive Intracellular DOX Release

Taking advantage of the watertight encapsulation of DOX into the hybrid plasmonic LNPs preventing the early cargo release or leakage in the natural physicochemical conditions, a pulse laser irradiation at the resonance (≈ 530 nm) of the hybrid plasmonic LNPs robustly promotes a stimuli-responsive intercellular release of the encapsulated DOX into the cancer cells (MDA-MB-231 adenocarcinoma breast cancer cell line). To examine the stimuli-responsive intracellular DOX release (Figure 2A), the cancer cells have been initially incubated with DOX-Au-LNPs. After removing the excess free LNPs, single-pulse laser irradiation was carried out by scanning the treated cells' target region ($500 \mu\text{m} \times 500 \mu\text{m}$) with the internalized DOX-Au-LNPs. By performing irradiation at the scanning speed of $50 \mu\text{m s}^{-1}$ and a repetition rate of 10 Hz (objective 10X with numerical aperture 0.13), each internalized DOX-Au-LNPs received a single pulse of at least $\approx 91\%$ of the peak fluence (the focused Gaussian beam by adjusting the objective on the target region, Section S.2, Supporting Information).

The single-pulse laser-triggered DOX release has occurred only in our integrated system by taking advantage of the internalized hybrid plasmonic LNPs ($50 \mu\text{g mL}^{-1}$ equal to $5 \mu\text{g mL}^{-1}$ of free DOX with a drug-to-lipid ratio of 0.1 wt/wt) and irradiation on the target region. Compared to the control systems, the single-pulse irradiation with the above-mentioned parameters on the target cells with the internalized DOX-loaded LNPs without AuNPs has not been effective. It showed a similar result to the region without irradiation and with hybrid plasmonic LNPs. A significant DOX release into the irradiated cells treated with hybrid plasmonic LNPs, seen as strong red fluorescence intensity in the cell nucleus, same as the DOX-only control group, was observed in all the strategies of Figure 2B. The single-pulsed laser irradiation alone has not been able to promote the DOX release in all control groups (no red fluorescence in Figure 2B in control groups). To obtain an optimal internalization window for DOX-Au-LNPs into the target cells (Figure 2B), different incubation

times from 15 min to 4 h have indicated a nonsignificant effect on the fluorescent intensity (20 h post-irradiation) of the irradiated cells due to the high-rate cellular uptake at the early stage of the incubation. A short incubation (15 min) of DOX-Au-LNPs ($50 \mu\text{g mL}^{-1}$) with the target cells has been sufficient for gaining a good internalization since the amount of the released DOX on the target cells, and diffusion in the nuclei was consistent compared to the longer incubation time (4 h). It may indicate a quick internalization and penetration of the DOX-Au-LNPs into the tumor microenvironment by overcoming biological barriers before being systematically washed away. These washed-away and non-irradiated DOX-loaded LNPs (DOX-LNPs) are made to be stable and remain intact after being internalized by healthy cells, thus not leading to cytotoxicity. In addition, the single-pulse irradiation performed before the washing step (after the LNPs incubation) has triggered a similar intracellular DOX release compared to the groups with the washing step, thereby indicating a minimal effect of the single-pulse irradiation on free DOX-Au-LNPs outside of the target cells. A short incubation time from the addition of nanocarriers to the washing step, preventing probable cellular damage to the healthy cells, provides a therapeutic amount of intercellular DOX release that can be triggered by performing single-pulse ns irradiation to the target cancer cells.

The stimuli-responsive intracellular release into target MDA-MB-231 cells, dynamically performed using nanosecond pulsed laser (scanning mode), have been evaluated using fluorescence microscopy after post-treatment incubation (20 h). As shown in Figure 3A, the laser scanning parameters, including different pitch sizes and velocities (condition-I: $10 \mu\text{m}$ with $100 \mu\text{m s}^{-1}$ and condition-II: $5 \mu\text{m}$ with $50 \mu\text{m s}^{-1}$) as well as pulse energies, have indicated a significant effect on the intracellular DOX release, and eventually accumulated into the nucleus (Figure S4, Supporting Information). Accordingly, the applied dynamic irradiation for condition-I and -II has provided an exposure of $> 91\%$ and $> 98\%$ of the peak fluence to the target region ($500 \mu\text{m} \times 500 \mu\text{m}$), respectively (Section S.2, Supporting Information). To eliminate non-specific intracellular DOX release and laser toxicity, a pulse energy threshold of $14.2 \mu\text{J}$ has been determined to effectively induce sixfold higher DOX release from DOX-Au-LNPs compared to the non-effective irradiation of the DOX-LNPs (without AuNPs) as illustrated in Figure 3A. Moreover, the reduction of the pitch size to $5 \mu\text{m}$ (condition-II) to fully cover the target region has enhanced up to 11-fold the DOX release from DOX-Au-LNPs compared to the irradiated DOX-LNPs (without AuNPs) exposed to the pulse energy of $14.2 \mu\text{J}$ (Figure 3B). Although all control groups (e.g., DOX-LNPs with and without irradiation) have not released their DOX cargo into the target cells due to the lack of the encapsulated AuNPs, the irradiation alone with more pulses per spot at higher fluence (e.g., $30 \mu\text{J}$) can probably damage the cells, prevent cell-membrane recovery and cause cytotoxicity.

To evaluate the cancer cell death caused by the stimuli-responsive release of DOX after the site-specific single pulse

Figure 1. Design, characteristics, and optical properties of DOX-Au-LNPs system. The average A) size, B) PDI, and C) zeta potential of the formulated DOX-Au-LNPs, DOX-LNPs, Au-LNPs, and LNPs. D) Four configurations with clustering of 5 nm AuNPs trapped inside of the LNPs; the most representative case corresponds to the top-left image (AuNPs within the junction of bilayers) (Cryo-TEM images were adapted with permission.^[22] Copyright 2022, American Chemical Society). The inset scale bar corresponds to 100 nm. E) The absorption spectrum of DOX-Au-LNPs, DOX-LNPs, Au-LNPs, LNPs, and DOX indicates the presence of AuNPs and DOX in the complex structure of hybrid plasmonic nanocarriers. F) Fluorescence spectra of DOX-Au-LNPs and DOX-LNPs indicating the DOX encapsulation (Ex/Em: 490/595 nm). All those spectra were measured at the equivalent concentration of DOX and the corresponding concentration of LNPs.

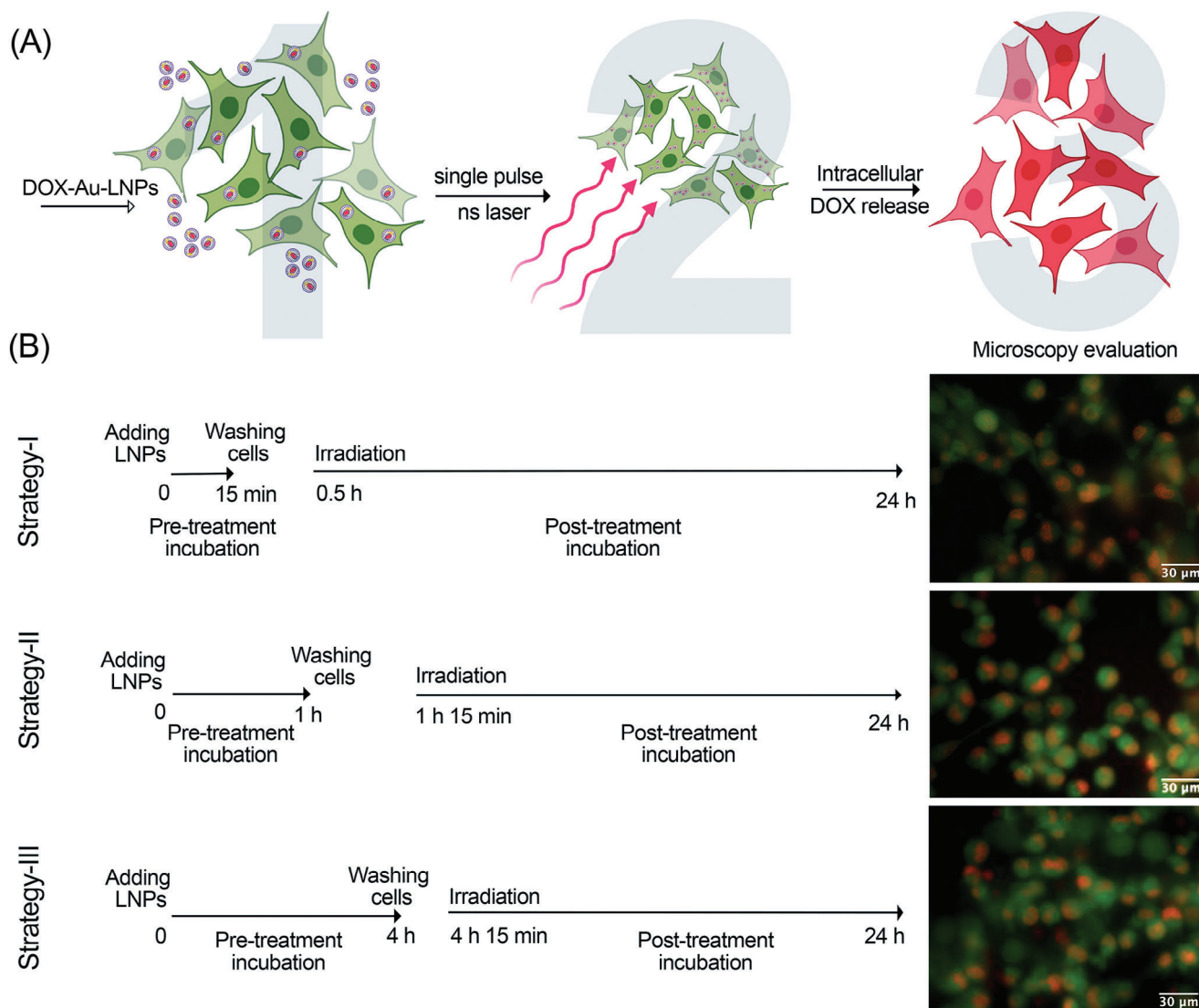


Figure 2. A) Representative schematic of stimuli-responsive intracellular DOX release from the internalized DOX-Au-LNPs following single pulse irradiation with pulsed ns laser at the plasmonic resonance 540 nm. B) Different strategies for the incubation (I: 15 min, II: 1 h, and III: 4 h) of DOX-Au-LNPs ($50 \mu\text{g mL}^{-1}$) with the target MDA-MB-231 cells have been taken place to gain an optimal cellular uptake for performing a highly efficient single-pulse ns irradiation. The fluorescence images in each strategy show the treated MDA-MB-231 cells incubated with DOX-Au-LNPs. The control DOX-LNPs with and without single-pulse irradiation are shown in Figures S1–S3, Supporting Information). The irradiation was performed with an objective 4X (NA 0.13), pulse energy of $19.7 \mu\text{J}$, velocity of $50 \mu\text{m s}^{-1}$, and pitch of $5 \mu\text{m}$. The green color shows calcein-AM stained cells, and the red indicates the released DOX.

laser irradiation, the irradiated MDA-MB-231 cells at the target region ($500 \mu\text{m} \times 500 \mu\text{m}$) have been stained with calcein-acetoxymethylester (calcein-AM) to indicate the viable cells (20 h post-treatment) under fluorescence microscopy. Accordingly, a significant decrease in the number of viable cells treated with DOX-Au-LNPs has been counted after the irradiation. Many of these irradiated cells with internalized DOX have been detached during the post-irradiation incubation (20 h), and no proliferation has been observed in this treated region compared to the control groups (treated cells with DOX-Au-LNPs without irradiation and DOX-LNPs with and without irradiation). As shown in Figure 3C, the irradiation of the cells treated with the DOX-Au-LNPs by following condition-II has reduced the cell viability

(detached cells) by 25% (pulse energy of $14.2 \mu\text{J}$) and 50% (pulse energy of $19.7 \mu\text{J}$). In addition, an intensive intracellular red fluorescence (tenfold) related to the released DOX from the DOX-Au-LNPs has been observed at the stronger pulse energy ($19.7 \mu\text{J}$) compared to the weaker ones. The dead and living cell imaging by propidium iodide (PI) and calcein-AM staining was performed after the irradiation on the different control samples to assess cell viability (Figure 3D). The control groups, including the irradiation alone and DOX-LNPs without AuNPs ($19.7 \mu\text{J}$ with condition-I and -II), have shown no significant difference in the number of viable cells before and after treatments, indicating that almost all the cells stayed alive. This integrated mechanism triggering the DOX release does not impact cell viability but only the

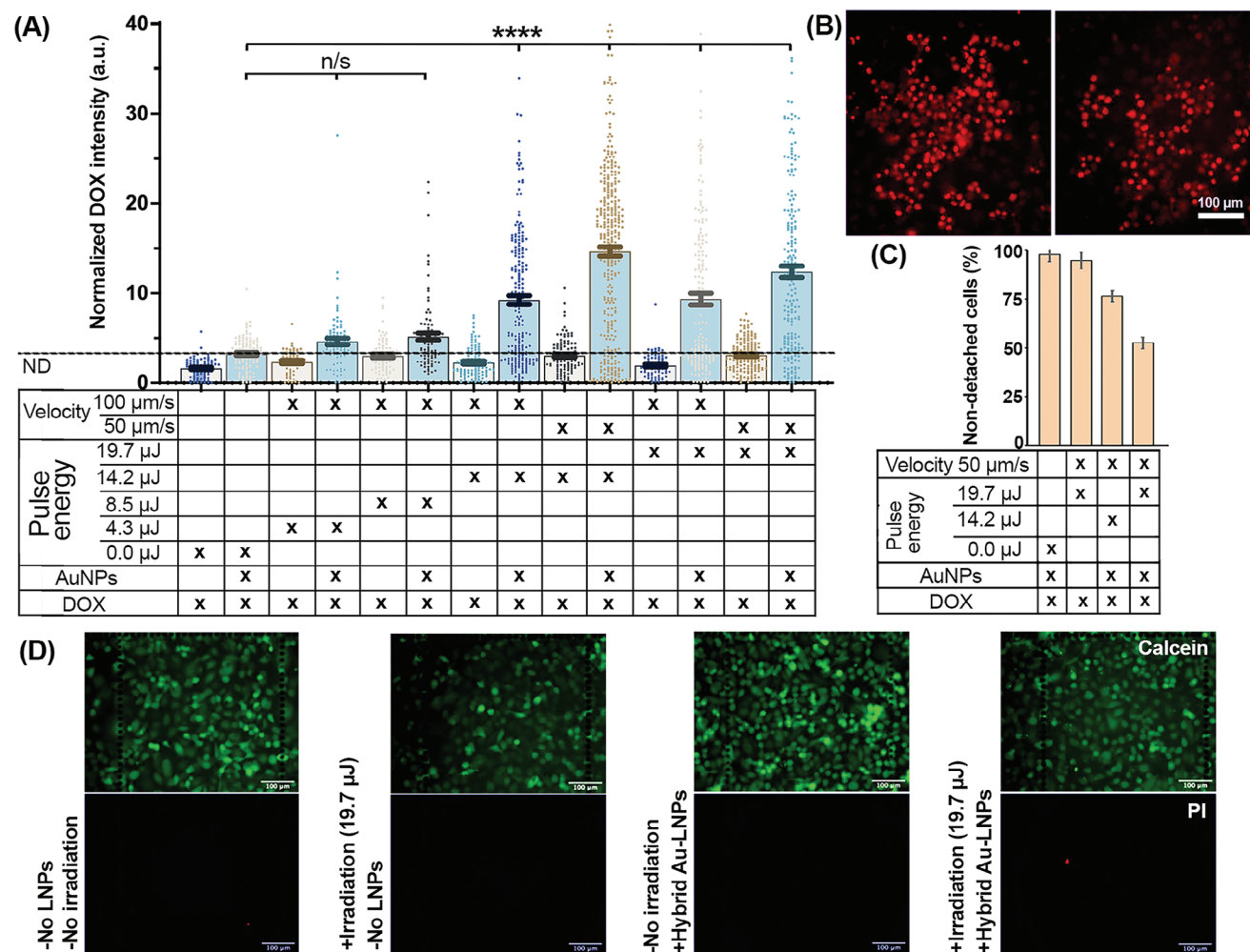


Figure 3. A) The normalized fluorescence intensity of the treated MDA-MB-231 cells (region: 500 $\mu\text{m} \times 500 \mu\text{m}$) incubated with the formulated DOX-Au-LNPs and DOX-LNPs (50 $\mu\text{g mL}^{-1}$) in different irradiation conditions. The groups with the same fluorescence intensity compared to the background have been shown and separated by a line (considered non-detected = ND fluorescence), and p-values were calculated based on the cells treated with DOX-Au-LNPs without irradiation. Statistically significant intracellular stimuli-responsive DOX release compared to the control is labeled **** $p < 0.0001$ and n/s: non-significant. B) The representative fluorescence images of the treated MDA-MB-231 cells incubated with DOX-Au-LNPs (50 $\mu\text{g mL}^{-1}$) and irradiated with pulse energy of 14.2 and 19.7 μJ , velocity 50 $\mu\text{m s}^{-1}$ (pitch size: 5 μm). The red color indicates the released DOX from DOX-Au-LNPs after the irradiation. C) The detachment percentage of the MDA-MB-231 cells incubated with DOX-Au-LNPs and DOX-LNPs and irradiated in different conditions after the post-treatment stage (20 h after the irradiation). D) The representative fluorescence images of MDA-MB-231 cells treated with control Au-LNPs without DOX (50 $\mu\text{g mL}^{-1}$) irradiated with a laser pulse energy of 19.7 μJ and compared with other control groups (without Au-LNPs in different irradiation conditions as well as the treated cells without the irradiation). Calcein-AM (green) and PI (red) staining indicate live/dead cells following the irradiation and the incubation with control Au-LNPs without DOX.

integrity of the liposome outer lamella for promoting the stimuli-responsive release of DOX at the specific region.

2.3. Numerical Simulation of Single Pulse Stimuli-Responsive DOX Release

To determine triggering mechanisms promoting the stimuli-responsive drug release from hybrid plasmonic NPs by ns laser radiation, the interaction of a single spherical AuNP (5 nm in diameter) with a single laser pulse has been numerically simulated. In this study, AuNP was assumed to either be surrounded by water or lie within a lipid bilayer comprised of DSPC/cholesterol

60:40. Note that PEG 1% influence was neglected, and the thermo-optical properties of DODAP molecule were assumed to be similar to those of DSPC. The geometries of the studied system are graphically represented in **Figure 4**. During the laser-NP interaction, thermodynamic transitions may occur for the AuNP and its surroundings (water of lipids) at characteristic temperatures. The thermal model here shall serve as a first-order approximation since such transitions are not considered. Collective heating effects have been considered, which are expected to result in higher local temperatures between adjacent AuNPs.

A two-temperature model coupled with a thermal diffusion equation has been employed (Section S.3, Supporting Information). The transient temperature increase within a control

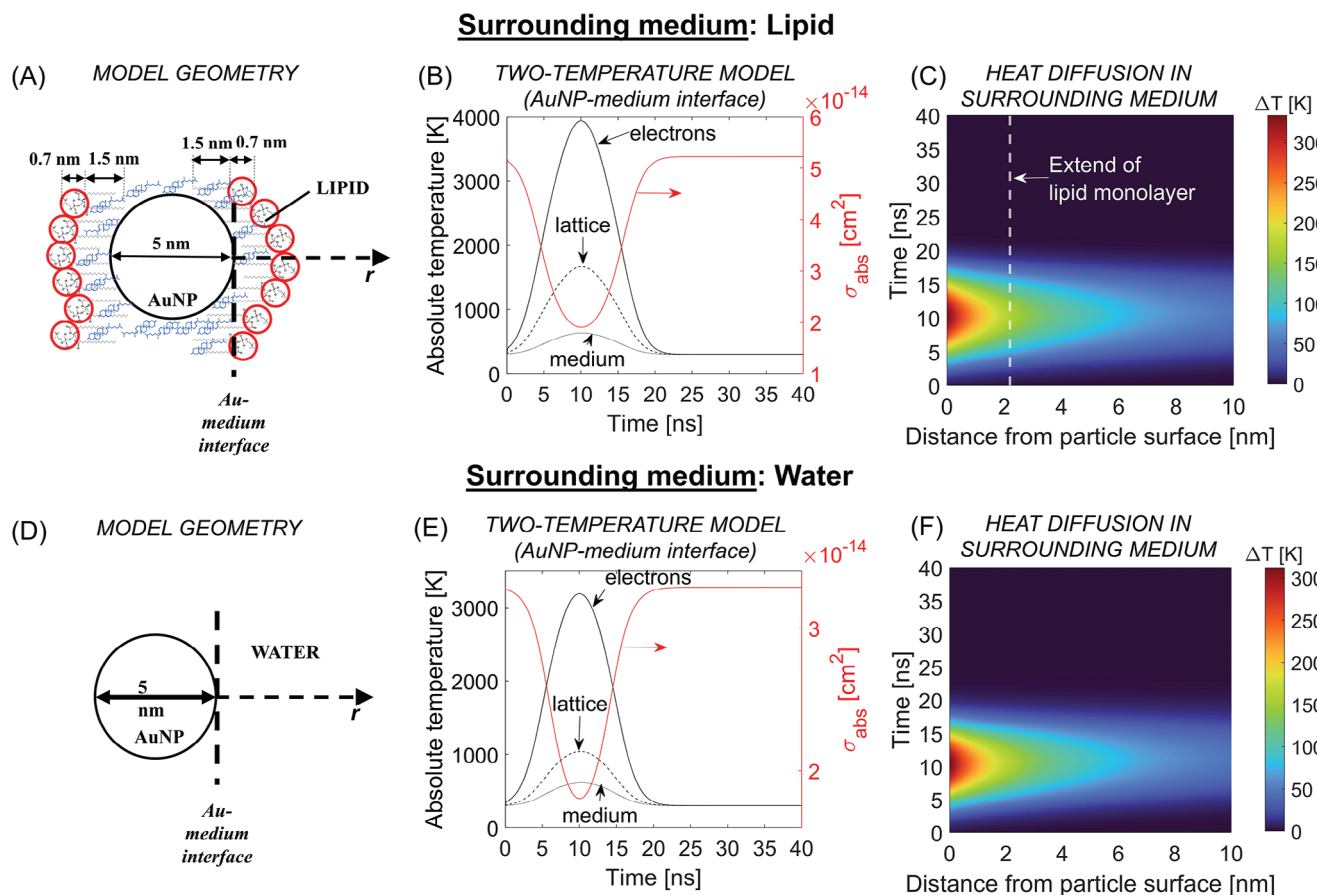


Figure 4. Model geometries and respective results of numerical simulations. The interaction of a single particle with a single nanosecond pulse is considered for two cases: a single AuNP is located within the lipid bilayer or in aqueous compartments of the oligomellar vesicles. Laser fluence $F \sim 1.6 \text{ J cm}^{-2}$. A,D) The geometry of the problem for lipid and water medium, respectively. B,E) Left-axes: the absolute temperature results of the two-temperature model at the interface of a single nanoparticle and the surrounding medium (lipid and water, respectively). Right-axes: the temporal evolution of the absorption cross-section of the particle. C,F) The spatiotemporal evolution of temperature transient increase in the surrounding medium.

volume was calculated at a fluence 1.6 J cm^{-2} (corresponding to a pulse energy of $14.2 \mu\text{J}$), as shown in Figure 3, at the estimated $16.5 \mu\text{m}$ $1/e^2$ beam spot radius), at which increased drug release triggered by laser radiation is observed experimentally. The simulation results shown in Figure 4 indicate that the calculated temperatures transiently exceed the onset of thermodynamic transitions of the Au and its surroundings. The melting point of bulk Au ($\approx 1370 \text{ K}$) is well exceeded when lipid is taken as the surrounding medium. Maximum temperatures of ≈ 630 or $\approx 615 \text{ K}$ are reached at the interface when lipid or water is taken as the surrounding medium, respectively. The system cools to room temperature within $\approx 10 \text{ ns}$ (following the pulse envelope).

In what follows, an absolute temperature of 600 K is taken as a reference to evaluate triggered drug release. Indeed, thermogravimetric analysis (heating from 50 to $700 \text{ }^\circ\text{C}$, heating rate $10^\circ\text{C min}^{-1}$) of DSPC/cholesterol/Dimethyldioctadecylammonium (DDAB) liposomes (6:4:1 molar ratio), has shown peak decomposition temperatures at ≈ 270 and $\approx 330 \text{ }^\circ\text{C}$ with $\approx 50\%$ weight loss.^[23] Furthermore, bubble nucleation reportedly occurs when a thin layer of $1\text{--}2 \text{ nm}$ of water crosses the spinodal temperature of water ($\approx 580 \text{ K}$) for particles $>10 \text{ nm}$. However, for smaller parti-

cles, the required value of overheated layer thickness is expected to increase further under the influence of Laplace pressure.^[24] Lastly, the absolute temperature of $\approx 500 \text{ K}$ is taken as a reference to evaluate the integrity of the encapsulated DOX. It has been shown that DOX typically undergoes substantial decomposition when heated beyond $220 \text{ }^\circ\text{C}$.^[25]

The effect of collective heating due to the clustering of AuNPs has been further considered (Figure 5; Section S.3, Supporting Information) to estimate the affected zones that exceed 600 and 500 K around a cluster of seven particles (average number of particles per cluster $\approx 6\text{--}7$, based on Cryo-TEM images; see Figure 1D top-left image being the most representative case where the AuNPs clusters are within the junction of bilayers). At laser fluence $F \approx 1.6 \text{ J cm}^{-2}$, depending on the type and orientation of a cluster, calculations have shown that 600 K temperature is transiently ($\approx 1 \text{ ns}$) reached at distances $d(T = 600 \text{ K}) \approx 3.8\text{--}10.5 \text{ nm}$ away from the cluster perimeter, exceeding the typical thickness of a single lipid bilayer ($\approx 4.2 \text{ nm}$). At the same fluence, the corresponding distance of 500 K temperature was estimated to vary between $d(T = 500 \text{ K}) \approx 8.7\text{--}18.1 \text{ nm}$ away from the cluster perimeter, which amounts for $7.6\text{--}15.8\%$ of the liposome hydrodynamic diameter. The calculation indicates that the encapsulated

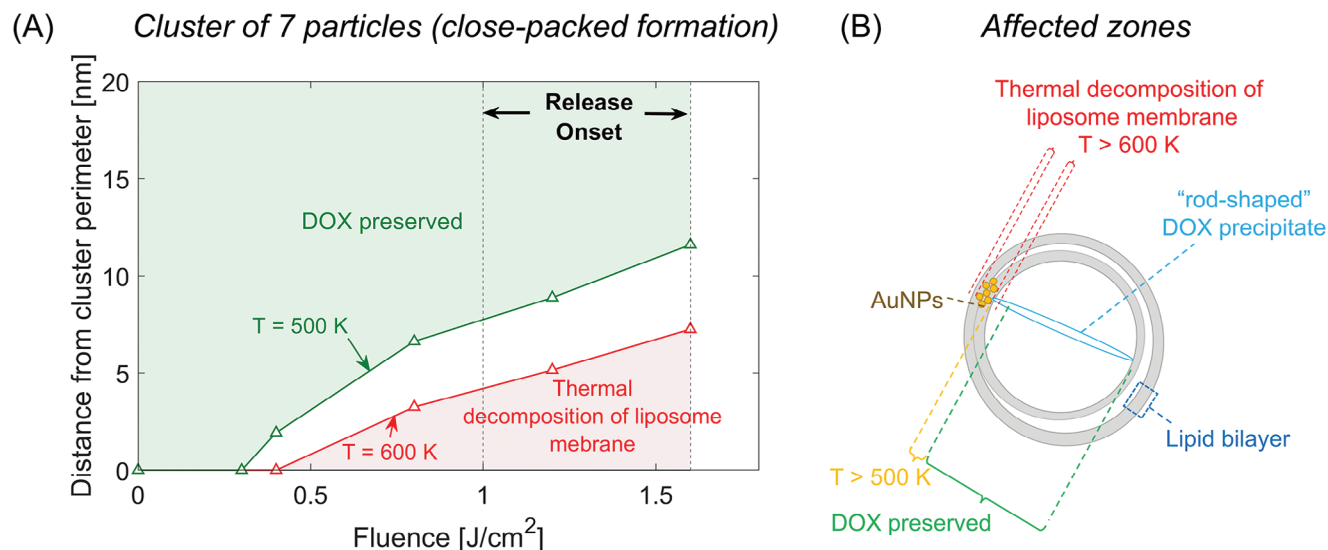


Figure 5. A) The affected zones around a cluster of seven particles, due to collective heating, as a function of input laser fluence F . The affected zones are defined by the maximum distance from the cluster perimeter over which a characteristic temperature is attained at the peak of the pulse. The red line $d(F, T = 600 \text{ K})$ corresponds to the distance at which a maximum absolute temperature of 600 K is attained, which demarcates the thermal decomposition of liposomes.^[23] Therefore, the latter effect expectedly occurs within the red area of the graph. The green line $d(F, T = 500 \text{ K})$ indicates the distance at which maximum absolute temperature of 500 K is attained, which demarcates the onset of thermal decomposition of DOX.^[25] Therefore, DOX integrity is expected preserved within the green area of the plot. B) Schematic representation of the affected zones under single pulse irradiation near the fluence threshold required for drug release.

DOX probably remains intact for the most part, while a portion (<15.8%) may undergo thermal degradation. Reportedly, thermogravimetric analysis of DOX has shown a 5% weight loss of the molecule in the range of 500–600 K within minutes of continuous heating.^[25] Thermal degradation of equal extent is yet unlikely within the nanosecond timescale, indicating that DOX would have kept its integrity after a single nanosecond irradiation.

Requiring experimentally a laser fluence $>1.6 \text{ J cm}^{-2}$ and highly localized temperature transients $>600 \text{ K}$ to obtain efficient and triggered drug release implies that it is necessary to destroy the lipid vesicles by a single pulse, rather than transiently and locally melting the lipid bilayers. In addition to numerical estimations, this conclusion is also supported by the following:

- 1) The employed DOX-LNPs are characterized as either bilamellar or oligolamellar vesicles.^[22] Cryo-TEM images (Figure 1D) based on our earlier study, describing in the fabrication protocol, have shown that, in principle, AuNPs are located at junctions of the inner and outer vesicles of a single lipid nanoparticle.^[22] However, as seen in Figure 1D, NPs may reside entirely within a bilayer of inner vesicles ($\approx 25\%$ of the population), or even at inner and intermediate aqueous compartments ($\approx 15\%$).
- 2) The permeability of the irradiated vesicles is altered only transiently after heating and recovers after cooling ($\approx 10 \text{ ns}$), provided that the vesicles are not fractured. For large unilamellar vesicles of pure DSPC,^[26] near the transition regime from gel to a liquid-disordered phase,^[27] permeability increases dramatically^[26,28] (as proven for DPPC vesicles),^[29] given abrupt structural changes. The transition is accompanied by significant changes in heat capacity δc_p , which in return affects the membrane permeability in nm/s as $P = c_0(T)$

+ $c_1(T)\delta c_p$, where $c_0(T)$ and $c_1(T)$ are monotonically increasing functions of temperature, related to thermal expansion of the lipid.^[29,30] Nonetheless, cholesterol lowers that transition below room temperature for pure lipids; therefore, the lamellae of the examined liposomes reside already at a liquid-ordered phase at room temperature.^[27] Further, cholesterol content significantly reduces the compressibility of the lipid and its permeability.^[28,30,31] By temperature increase (laser-induced heating of AuNPs) the liposomes are expected to undergo a transition from liquid-ordered toward liquid-disordered phase with negligible δc_p .^[26,27,32] We estimate the permeability of the liposomes studied here up to $\approx 400 \text{ K}$ (at their full lateral thickness); for instance, the order of magnitude of permeation rate k of fluorescent biomolecules through DPPC vesicles of $\approx 100 \text{ nm}$ is reported $\approx 10^{-3} \text{ s}^{-1}$, maintained beyond the gel to liquid-disordered transition.^[29] This can be considered an upper limit value since, generally, cholesterol prevents abrupt changes in permeability and reduces its value. Assuming $P \approx kr/3$ ^[28] (r is the size of the vesicle), a maximum transient permeability $P < 0.1 \text{ nm s}^{-1}$ is estimated for the lipid vesicles studied here when heated to the liquid-disordered regime (total release of content in $< 10^3 \text{ s}$ through the unilamellar vesicle).

- 3) At higher temperatures ($\approx 400\text{--}600 \text{ K}$), vaporization of aqueous compartments near heated nanoparticles is expected. Thereby, the lipid bilayer surroundings are transiently dehydrated, which raises its critical points^[33] and hinders further increase of the membrane permeability. For instance, thermotropic melting (to liquid-ordered phase) of pure, anhydrous (or monohydrate) DSPC occurs around $\approx 390 \text{ K}$, and isotropic melting (to liquid-disordered phase) around $\approx 500 \text{ K}$.^[33a] Furthermore, a water vapor nanobubble can be nucleated when a thin water layer of $\approx 1\text{--}2 \text{ nm}$ is heated beyond $\approx 600 \text{ K}$.^[24] Notably, this

temperature is close to the decomposition temperatures of free cholesterol and heptadecane.^[34] Thus, the lipid bilayer surrounding AuNPs is expected to undergo thermo-mechanical decomposition when transiently overheated beyond 600 K at their full extent (≈ 4.4 nm lateral thickness for a single bilayer).

Taken together, following the laser-induced heating of AuNPs, it is reasonable to assume that the exchange rate of DOX through localized overheated (liquid-disordered) lipids is unlikely to change dramatically unless all vesicles of the bilamellar or oligolamellar liposomes are disrupted. Drug release rates will then be governed by the diffusion coefficient of the DOX precipitates in water (or solutions with a similar viscosity). In other words, a volatile interaction must be triggered; however, there is little doubt, according to calculations, that drug release is mediated by either explosive vaporization of thin water layers adjacent to AuNPs (or clusters of AuNPs) or thermo-mechanical decomposition of overheated lipid bilayers. Furthermore, due to the clustered AuNPs, the temperature increase is highly localized around the cluster, thus preserving the integrity of the encapsulated DOX inside the LNPs (e.g., located at the aqueous core).

3. Conclusion

This study demonstrates a highly accurate stimuli-responsive anticancer DOX release from hybrid plasmonic LNPs by single-pulsed laser irradiation. A single ns pulse in the resonance of AuNP clustered into the internal membrane of LNPs has been sufficient to locally decompose the liposomes, thus releasing the encapsulated DOX into the target cells. The laser irradiation (pulse energy 14.2 μJ) of the target cells with the internalized DOX-Au-LNPs enables an 11-fold increase in the intracellular DOX release compared with control cells (non-irradiated cells and irradiated ones incubated with DOX-LNPs without AuNPs in their structure). Compared to the control groups, these irradiation conditions have induced site-specific cell death in >50% of the irradiated cells (pre-treated with DOX-Au-LNPs). Numerical simulations suggest that a single nanosecond pulse results in a localized temperature increase near the AuNPs, inducing the thermal decomposition of adjacent lipid lamellae. Thus, the release of the DOX into the cell rapidly occurs and is governed by the diffusion coefficient of the molecule into the surrounding medium. Furthermore, this temperature increase has been sufficiently localized in space and time to preserve the DOX integrity before its release. While this proof-of-concept study has been experimentally demonstrated for the interaction between 5 nm AuNPs and pulsed ns laser (λ : 527 nm), the general approach can be extended to irradiation wavelengths in the near-infrared by using alternative types of plasmonic nanostructures, such as small nanorods. In our view, the single laser pulse-based stimuli-responsive release of DOX on the internalized DOX-Au-LNPs paves the way for both rapid and localized delivery of chemotherapeutics at deceased sites, thereby limiting side effects to non-irradiated healthy tissue.

4. Experimental Section

Cell culture: MBA-MD-231 cells (ATCC, Manassas, Virginia) were grown in Dulbecco's Modified Eagle Medium (DMEM, Thermo Fisher

Scientific, Waltham, Massachusetts) medium supplemented by 10% Fetal Bovine Serum (FBS, Life Technologies, Carlsbad, California), 1% Penicillin/Streptomycin (Life Technologies) and Glutamine amino acid antibiotics in 75 cm^2 polystyrene flasks (Sarstedt AG & Co., Germany). Cells were incubated in a 5% CO_2 , 37 °C environment.

Formulation of LNPs: Different formulations of liposomes (LNPs, DOX-LNPs, Au-LNPs, and DOX-Au-LNPs) were prepared by following our established T-tube protocol.^[22] Briefly, DODAP, DSPC, and PEG-DSPE were obtained from Avanti Polar Lipids (Alabaster, Alabama). Cholesterol and ammonium sulfate (AS) were purchased from Sigma-Aldrich (St. Louis, Missouri). DOX was bought from Cayman Chemicals (Ann Arbor, Michigan). Spherical AuNPs (5 nm diameter, particle concentration 5.5×10^{13} particles/mL) were provided by Ted Pella, Inc. (Redding, California) as aqueous dispersions. For the formation, for example, of DOX-Au-LNPs, a solution composed of DODAP, DSPC, and PEG-DSPE at a volume ratio of 10/49/40/1 had been prepared and formulated by mixing them in ethanol buffer with an aqueous phase containing AuNPs (Au/lipid concentration of 2.2×10^{13} particles/ μmol). The aqueous AS (450 mM) was added to the prepared lipid/AuNPs dispersion and dialyzed (dialysis membrane, cutoff 12–14 kDa, Spectrum Laboratories, Rancho Dominguez, California) against PBS to remove the ethanol and untrapped AS until reached pH 7.4. To encapsulate DOX into the Au-LNPs, the concentrated AS-containing Au-LNPs (10 mg mL^{-1} of lipid) were mixed with the DOX solution (0.1 wt/wt DOX-to-lipid ratio corresponding to 1 mg/mL of DOX) and incubated at 60 °C. After removing the free DOX, the loading efficiency was determined by analyzing the fluorescence intensity (excitation 480 nm and emission 590 nm) of the isopropanol-treated DOX-Au-LNPs (for obtaining 100% of DOX release) with a PerkinElmer LS50 fluorimeter (Perkin Elmer, Waltham, Massachusetts).

Absorbance and Fluorescence Quantification of LNPs: UV-visible spectra of LNPs were obtained using an Epoch spectrometer from BioTek Company (Winooski, Vermont). Samples were placed in 96-well plates holding a volume of 300 μL . Each measurement was performed with a working volume of 300 μL . Fluorescence spectra were obtained with a Shamrock spectrometer coupled with an ANDOR Newton camera from Oxford Instruments (Abingdon, UK). This spectrometer was mounted at the output of a microscope, which could be used to obtain spectra of small objects such as single nanoparticles. An objective, 10X, with a numerical aperture 0.3 was used to acquire the spectra with a fluorescence cube composed of 2 bandpass filters. This cube allowed to observe only the fluorescence spectrum. The cube comprises a bandpass filter from 505 to 555 nm, used for the excitation, and a bandpass filter from 570 to 620 nm, implemented for the emission (Nikon, Minato City, Tokyo, Japan). The light source used was "white" mercury.

Zeta Potential and Dynamic Light Scattering (DLS) Measurement: DLS measurements (average size and polydispersity index) and zeta potential measurements of LNPs were performed on a Zetasizer nano ZS (Malvern, UK). The different LNPs (0.1 mg mL^{-1}) were diluted in phosphate-buffered saline (PBS) from GIBCO (Thermo Fisher Scientific Inc.). The obtained solutions were placed in folded capillary zeta cells (Malvern, UK) to perform all the measurements with the software provided by Malvern.

Cryo-Electron Transmission Microscopy of LNPs: Cryo-electron transmission microscopy images (Cryo-TEM) of DOX-Au-LNPs were acquired on FEI Tecnai G20 TEM (TEI, Hillsboro, Oregon). The samples and images were prepared and taken at the UBC Bioimaging Facility (British Columbia, CA). Before imaging, the samples were concentrated at 20 mg mL^{-1} . An aliquot of 3–5 μL obtained was placed on a glow-discharged copper grid in an FEI Mark IV Vitrobot. It was then put into liquid ethanol to freeze and generate vitreous ice. Until imaging, the sample was put in liquid nitrogen. Imaging by TEM was performed at 200 kV in low dose mode, using a bottom mount FEI high-resolution CCD camera with an under-focus of 2–4 μm .

Samples Preparation Before the Laser Irradiation: Irradiations were performed on samples incubated in Ibidi μ -wells grid-500 plates (Munich, Germany) featuring $500 \mu\text{m} \times 500 \mu\text{m}$ grids to facilitate irradiation. 300 μL of cells were incubated at 2.5×10^4 cells mL^{-1} . After 2 days of incubation, LNPs were added to the cells at $5 \mu\text{g mL}^{-1}$ DOX (i.e., 50 $\mu\text{g mL}^{-1}$ lipid).

The LNPs were first diluted in the culture medium used before addition to the cells at the concentration of 50 $\mu\text{g mL}^{-1}$.

Laser Irradiation: The nanosecond laser used was a Quanta 1 from Quantum Light Instruments (Vilnius, Lithuania) to perform the ultrafast irradiations. The characteristics of the laser are a wavelength of 527 nm, pulse time of 7.7 ns, and repetition rate of 10 Hz. The samples were mounted on a microscope with a motorized plate (Proscan III, Prior Scientific, Rockland, Massachusetts) that could easily be controlled via LabView software to scan the sample. During irradiations, the plate containing the cells was placed in a portable incubator, allowing the cells to be maintained in a 37 °C environment with 5% CO₂. A Nikon 4X Fluor plane objective with a numerical aperture of 0.13 was used for the irradiations. The $1/e^2$ radius of the beam at the focal plane was estimated to be 16.5 μm .

Cells Staining: Calcein-AM and PI were purchased from Thermo Fisher Scientific to assess cell viability in samples without DOX. PI was added to the cells at a concentration of 6.3 μM . Calcein-AM staining (0.5 μM) was used to image cellular membranes in all samples and to assess cell viability. After a 30 min of incubation with the fluorophores, cells were washed twice with culture medium before leaving them in the medium (300 μL) used for growth.

Fluorescence Imaging Process: Red fluorescence images, that is, DOX and PI fluorescence, were acquired using a Cy3 filter (Nikon), with an excitation between 513 and 556 nm and an emission between 570 and 613 nm. Calcein-AM images were obtained using a green fluorescence filter from Nikon. A white light (X-Cite 120LED from Excelitas, Waltham, Massachusetts) was used with a Q Click Q imaging camera (Teledyne Photometrics, Tucson, Arizona) to obtain the fluorescence images. Two objectives (Nikon) were used to acquire the images: i) 20X, plan Fluor, with a 0.45 numerical aperture, and ii) 60X oil objective, with a numerical aperture from 0.5 to 1.25.

Quantification of Fluorescence Intensity: Quantification of fluorescence intensity was conducted using ImageJ software. All the images were taken with the same acquisition parameters. No adjustments were performed on the images for the intensity calculation. The average intensity of the red fluorescence of each nucleus was measured in different groups in the working / treated area of 500 $\mu\text{m} \times 500 \mu\text{m}$. The obtained value was normalized by subtracting the autofluorescence and background of each group. This value was considered as the minimal fluorescence measured. The total average of the normalized intensity was individually presented to statistically evaluate the performance of each group.

Quantification of Cell Death: Cells counting was performed using ImageJ software, using images acquired with a 20X objective before and after post-treatment staining with calcein-AM. This staining protocol removes all the dead cells due to DOX, detached from the plate. The ratio of the counting before and after staining in a given group was, therefore, representative of cell viability. Note that PI staining for the dead cell analysis due to overlapping its emission wavelength with that of DOX had not been used for the samples treated with DOX-loaded nanocarriers.

Statistical Analysis: The difference across multiple groups was statistically analyzed with GraphPad Prism software based on one-way non-parametric Kruskal-Wallis ANOVA of unpaired groups followed by Dunn's statistical hypothesis testing or two-stage set-up methods of Benjamini, Krieger, and Yekutieli for controlling the false discovery rate. p values were considered statistically significant, as n/s: not-significant, * $p < 0.05$, ** $p < 0.01$, *** $p < 0.001$, and **** $p < 0.0001$.

Supporting Information

Supporting Information is available from the Wiley Online Library or from the author.

Acknowledgements

A.U. and L.A. contributed equally to this work. The authors thank the NanoCore facilities from the University of British Columbia for providing different LNP formulations and the Nanomedicine Innovation Network for financial support. Schematics created with BioRender.com

M.H.K. Current address: Center for Translational Cancer Research (TranslaTUM), Heinz-Nixdorf-Chair for Biomedical Electronics, Klinikum rechts der Isar, Technische Universität München (TUM), Munich, Germany.

Conflict of Interest

The authors have declared no conflicts of interest.

Data Availability Statement

The data that support the findings of this study are available from the corresponding author upon reasonable request.

Keywords

lipid nanoparticles, nanosecond pulsed laser, plasmonic gold nanoparticles, single pulse perforation, stimulus-responsive drug release, targeted drug delivery

Received: July 4, 2023
Revised: October 19, 2023
Published online:

- [1] K. Park, *ACS Nano* **2013**, *7*, 7442.
- [2] O. Tacar, C. R. Dass, *J. Pharm. Pharmacol.* **2013**, *65*, 1577.
- [3] M. Ibrahim, W. H. Abuwatfa, N. S. Awad, R. Sabouni, G. A. Hussein, *Pharmaceutics* **2022**, *14*, 254.
- [4] P. Liu, G. Chen, J. Zhang, *Molecules* **2022**, *27*, 1372.
- [5] S. Bandak, A. Ramu, Y. Barenholz, A. Gabizon, *Pharm. Res.* **1999**, *16*, 841.
- [6] a) I. Ahmad, S. Ahmed, Z. Anwar, M. A. Sheraz, M. Sikorski, *Int. J. Photoenergy* **2016**, *2016*, 8135608; b) G. Ioele, M. De Luca, A. Garofalo, G. Ragno, *Drug Deliv.* **2017**, *24*, 33.
- [7] a) Y. Lee, D. H. Thompson, *Nanomed. Nanotechnol.* **2017**, *9*, e1450; b) J. Li, X. Wang, T. Zhang, C. Wang, Z. Huang, X. Luo, Y. Deng, *Asian J. Pharm. Sci.* **2015**, *10*, 81; c) S. Simões, V. Slepushkin, N. Düzgünes, M. C. Pedroso De Lima, *Biochim. Biophys. Acta Biomembr.* **2001**, *1515*, 23.
- [8] A. Mayer, S. K. Sharma, B. Tolner, N. P. Minton, D. Purdy, P. Amlot, G. Tharakan, R. H. J. Begent, K. A. Chester, *Br. J. Cancer.* **2004**, *90*, 2402.
- [9] a) T. M. Allen, P. R. Cullis, *Adv. Drug Delivery Rev.* **2013**, *65*, 36; b) S. Bibi, E. Lattmann, A. R. Mohammed, Y. Perrie, *J. Microencapsul.* **2012**, *29*, 262.
- [10] a) W. Chen, E. M. Goldys, W. Deng, *Prog. Lipid Res.* **2020**, *79*, 101052; b) D. Miranda, J. F. Lovell, *Bioeng. Transl. Med.* **2016**, *1*, 267; c) A. Ishii, Y. Hiruta, D. Heinemann, A. Heisterkamp, H. Kanazawa, M. Terakawa, *J. Biophotonics* **2017**, *10*, 1723; d) M. Hasanzadeh Kafshgari, L. Agiotis, I. Largillière, S. Patskovsky, M. Meunier, *Small* **2021**, *17*, 2007577.
- [11] a) A. Heisterkamp, *Opt. Photonik* **2010**, *5*, 38; b) F. Salehpour, P. Cassano, N. Rouhi, M. R. Hamblin, L. De Taboada, F. Farajdokht, J. Mahmoudi, *Photobiomodul. Photomed. Laser Surg.* **2019**, *37*, 581.
- [12] a) H. Xiong, X. Li, P. Kang, J. Perish, F. Neuhaus, J. E. Ploski, S. Kroener, M. O. Ogunyankin, J. E. Shin, J. A. Zasadzinski, H. Wang, P. A. Slesinger, A. Zumbuehl, Z. Qin, *Angew. Chem., Int. Ed.* **2020**, *59*, 8608; b) J. E. Shin, M. O. Ogunyankin, J. A. Zasadzinski, *Sci. Rep.* **2020**, *10*, 1706; c) L. J. E. Anderson, E. Hansen, E. Y. Lukianova-Hleb, J. H. Hafner, D. O. Lapotko, *J. Control. Release* **2010**, *144*, 151; d) G. Wu, A. Mikhailovsky, H. A. Khant, C. Fu, W. Chiu, J. A. Zasadzinski, *J. Am. Chem. Soc.* **2008**, *130*, 8175.

- [13] a) K. Zhu, Z. Zhu, H. Zhou, J. Zhang, S. Liu, *Chin. Chem. Lett.* **2017**, 28, 1276; b) J. Hu, T. Wu, G. Zhang, S. Liu, *J. Am. Chem. Soc.* **2012**, 134, 7624.
- [14] a) A. Dagallier, E. Boulais, C. Boutopoulos, R. Lachaine, M. Meunier, *Nanoscale* **2017**, 9, 3023; b) A. Nsamela Matombi, M. Hasanzadeh Kafshgari, L. Wang, S. Patskovsky, D. Trudel, M. Meunier, *ACS Appl. Nano Mater.* **2020**, 3, 4171; c) A. Hatef, B. Darvish, A. Dagallier, Y. R. Davletshin, W. Johnston, J. C. Kumaradas, D. Rioux, M. Meunier, *J. Phys. Chem. C* **2015**, 119, 24075; d) R. Lachaine, É. Boulais, M. Meunier, *ACS Photonics* **2014**, 1, 331; e) L. Wang, M. Hasanzadeh Kafshgari, M. Meunier, *Adv. Funct. Mater.* **2020**, 30, 2005400.
- [15] a) Z. Wang, M. Zhan, W. Li, C. Chu, D. Xing, S. Lu, X. Hu, *Angew. Chem., Int. Ed.* **2021**, 60, 4720; b) Z. Wang, M. Zhan, X. Hu, *Chem. - Eur. J.* **2022**, 28, e202200042.
- [16] a) K. Koga, T. Tagami, T. Ozeki, *Colloids Surf. A: Physicochem. Eng. Asp.* **2021**, 626, 127038; b) K. Hou, M. Bao, C. Xin, L. Wang, H. Zhang, H. Zhao, Z. Wang, *Adv. Powder Technol.* **2020**, 31, 3640; c) Z. Kautzka, S. Clement, E. M. Goldys, W. Deng, *Int. J. Nanomed.* **2017**, 12, 969; d) K. Kim, K. S. Oh, D. Y. Park, J. Y. Lee, B. S. Lee, I. S. Kim, K. Kim, I. C. Kwon, Y. K. Sang, S. H. Yuk, *J. Control. Release.* **2016**, 228, 141; e) Y. Li, D. He, J. Tu, R. Wang, C. Zu, Y. Chen, W. Yang, D. Shi, T. J. Webster, Y. Shen, *Nanoscale* **2018**, 10, 8628.
- [17] A. Veeren, M. O. Ogunyankin, J. E. Shin, J. A. Zasadzinski, *Pharmaceuticals* **2022**, 14, 701.
- [18] a) J. Jiang, S. Liu, C. Wang, H. Zhang, *J. Nanomater.* **2018**, 2018, 3568190; b) M. Mathiyazhakan, P. K. Upputuri, K. Sivasubramanian, A. Dhayani, P. K. Vemula, P. Zou, K. Pu, C. Yang, M. Pramanik, C. Xu, *Sci. China Mater.* **2016**, 59, 892.
- [19] K. Sivasubramanian, M. Mathiyazhakan, C. Wiraja, P. K. Upputuri, C. Xu, M. Pramanik, *J. Biomed. Opt.* **2017**, 22, 041007.
- [20] C. Wiraja, M. Mathiyazhakan, F. Movahedi, P. K. Upputuri, Y. Cheng, M. Pramanik, L. Yang, D. L. Becker, C. Xu, *Bioeng. Transl. Med.* **2016**, 1, 357.
- [21] X. Li, Z. Che, K. Mazhar, T. J. Price, Z. Qin, *Adv. Funct. Mater.* **2017**, 27, 1605778.
- [22] I. V. Zhigaltsev, Y. Y. C. Tam, J. A. Kulkarni, P. R. Cullis, *Langmuir* **2022**, 38, 7858.
- [23] G. Jose, Y.-J. Lu, H.-A. Chen, H.-L. Hsu, J.-T. Hung, T. S. Anilkumar, J.-P. Chen, *J. Magn. Magn. Mater.* **2019**, 474, 355.
- [24] J. Lombard, T. Biben, S. Merabia, *J. Phys. Chem. C* **2017**, 121, 15402.
- [25] B. Manocha, A. Margaritis, *J. Nanomater.* **2010**, 2010, 780171.
- [26] T. Lu, T. L. M. Ten Hagen, *J. Control. Release* **2017**, 247, 64.
- [27] a) N. Tamai, M. Uemura, T. Takeichi, M. Goto, H. Matsuki, S. Kaneshina, *Biophys. Chem.* **2008**, 135, 95; b) D. Marsh, *Biochim. Biophys. Acta Biomembr.* **2010**, 1798, 688.
- [28] R. Lawaczek, *J. Membr. Biol.* **1979**, 51, 229.
- [29] A. Blicher, K. Wodzinska, M. Fidorra, M. Winterhalter, T. Heimburg, *Biophys. J.* **2009**, 96, 4581.
- [30] J. F. Nagle, H. L. Scott, *Biochim. Biophys. Acta Biomembr.* **1978**, 513, 236.
- [31] D. Papahadjopoulos, S. Nir, S. Ohki, *Biochim. Biophys. Acta Biomembr.* **1972**, 266, 561.
- [32] P. F. Almeida, F. E. Carter, K. M. Kilgour, M. H. Raymonda, E. Tejada, *Langmuir* **2018**, 34, 9798.
- [33] a) D. Chapman, R. M. Williams, B. D. Ladbroke, *Chem. Phys. Lipids* **1967**, 1, 445; b) S. K. Owusu-Ware, B. Z. Chowdhry, S. A. Leharne, M. D. Antonijevic, *J. Therm. Anal. Calorim.* **2017**, 127, 415.
- [34] R. A. Lewis, *Hawley's Condensed Chemical Dictionary*, John Wiley & Sons, New Jersey, USA **2016**.